JOURNAL OF MATERIALS SCIENCE **40** (2005) 3185–3190

# Oxygen diffusion blocking of single grain boundary in yttria-doped zirconia bicrystals

T. NAKAGAWA
*Institute of Engineering Innovation (Department of Materials Engineering), The University of Tokyo, 2-11-16, Yayoi, Bunkyo-ku, Tokyo 113-8656, Japan*

I. SAKAGUCHI
*Advanced Materials Laboratory, National Institute for Materials Science, 1-1, Namiki, Tsukuba, Ibaraki 305-0044, Japan*

N. SHIBATA, K. MATSUNAGA, T. YAMAMOTO
*Institute of Engineering Innovation (Department of Materials Engineering), The University of Tokyo, 2-11-16, Yayoi, Bunkyo-ku, Tokyo 113-8656, Japan*

H. HANEDA
*Advanced Materials Laboratory, National Institute for Materials Science, 1-1, Namiki, Tsukuba, Ibaraki 305-0044, Japan*

Y. IKUHARA
*Institute of Engineering Innovation (Department of Materials Engineering), The University of Tokyo, 2-11-16, Yayoi, Bunkyo-ku, Tokyo 113-8656, Japan*

Yttrium-doped zirconia bicrystals with [001] symmetric tilt Σ5 grain boundaries were fabricated by a diffusion bonding technique, and oxygen diffusion behavior across the grain boundary was measured by secondary ion mass spectrometry (SIMS), tracing $^{18}O$ isotope. It was found that the $^{18}O$ fraction across the boundary exhibited explicit decrease around the boundary plane, indicating that the oxygen-diffusion is blocked by the presence of the Σ5 grain boundary. This is the first experimental detection of oxygen diffusion blocking at a single grain boundary in zirconia ceramics. From high-resolution transmission electron microscopy observations and energy dispersive X-ray spectroscopy analysis, neither amorphous layers nor Si impurity segregation were found at the grain boundary. The grain boundary blocking effect of the Σ5 boundary must be an intrinsic feature arising from its core structure and yttrium solute segregation of the grain boundary.


## 1. Introduction

Zirconia ($ZrO_2$) with the cubic fluorite structure, stabilized with dopants such as $Y^{3+}$and $Sc^{3+}$, exhibits high electrical conductivity, which is suitable for applications as solid electrolytes in fuel cells. Electrical conductivity of $ZrO_2$ materials mainly arises from oxygen diffusion via vacancies, which are generated by doped aliovalent cations due to maintaining charge neutrality of the doped material system. It is known that the oxygen ionic conductivity strongly depends on dopant types and their concentrations, indicating that detailed chemical interactions between oxygen vacancies and dopants play a crucial role for oxygen-ion diffusivity [1–3]. The overall oxygen ionic conductivity of $ZrO_2$ is also affected by microstructures in the polycrystalline state [4, 5]. In this case, it can be speculated that grain boundaries have a great influence on the motion of oxygen vacancies, due to particular grain-boundary structures and/or dopant/impurity segregation [5–7].

So far, a number of experimental studies have been performed to understand the effects of grain boundaries on the ionic conductivity of $ZrO_2$. Aoki *et al.* investigated a correlation between grain size and ionic conductivity in 15 mol% CaO-stabilized $ZrO_2$ with different grain sizes, and showed that oxygen ionic conductivities across the grain boundaries readily decreased with increasing grain sizes [8]. Their results indicate that Si enrichment at the grain boundaries gives rise to blocking of oxygen diffusion across the grain boundaries. Also, Badwal *et al.* pointed out that siliceous intergranular phases in YSZ act as barriers for oxygen transport across the grain boundaries [4]. Therefore, Si impurities at zirconia grain boundaries have been considered as a major reason to hamper fast diffusion of oxygen ions through the microstructures. In contrast, Guo *et al.* [9] showed a blocking effect of silicate-free grain boundaries on oxygen diffusion in 8 mol% YSZ, and explained their observed results were based on the space charge effect [10], in which

oxygen-vacancy depletion takes place around the grain boundaries.

As mentioned above, oxygen diffusivity in polycrystalline $ZrO_2$ is closely related to complicated factors arising from grain boundary structures and chemistry. Moreover, grain boundary geometries against a flow of current are also important, because it is thought that grain boundary resistance to oxygen diffusion in $ZrO_2$ may be different for the cases that a grain boundary plane lies parallel or perpendicular to a flow of current. However, grain boundaries in usual polycrystalline $ZrO_2$ have various kinds of grain-boundary characters and chemistry, forming grain boundary networks through the microstructures. Therefore, it is difficult to understand a detailed mechanism of grain boundary effects on oxygen-ion conduction in $ZrO_2$ materials by conventional experiments using polycrystalline materials. It is desirable to investigate oxygen diffusion behavior at individual grain boundaries. For this purpose, bicrystal experiments are advantageous, since bicrystals have single grain boundaries with well-defined grain boundary characters. In addition, atomic structures and dopants/impurities segregation at grain boundaries in bicrystals can also be quantitatively revealed in combination with high-resolution transmission electron microscopy (HRTEM) and chemical analyses using nanometer-sized electron probes.

For YSZ, several researchers studied particular grain boundaries in YSZ bicrystals, and found characteristic atomic structures and Y segregation behavior around grain-boundary cores, depending on grain boundary characters [11–13]. In contrast, bicrystals have been also used to investigate grain boundary diffusion in oxides such as MgO and $Al_2O_3$ [14–18]. These results showed substantial enhancement of ionic diffusion at grain boundaries, and strong dependence of diffusion on grain boundary characters. Therefore, bicrystal experiments, in which grain boundary character is systematically changed, can provide direct evidence of grain-boundary blocking effects on oxygen diffusion in $ZrO_2$ materials.

In this study, yttrium-doped zirconia bicrystals with the [001] symmetric tilt $\Sigma 5$ grain boundary were fabricated by a diffusion bonding technique, and the grain-boundary atomic structure was investigated by HRTEM. Furthermore, the behavior of oxygen diffusion was directly examined across a single grain boundary by SIMS measurements.

## 2. Experimental procedure

In this study, $\Sigma 5$ symmetric tilt grain boundary with a rotation axis of [001] was selected as a model grain boundary. Fig. 1 shows the grain-boundary geometry of YSZ bicrystals with a misorientation angle of $2\theta$. The $\Sigma 5$ boundary can be obtained by a tilt angle of 53.2° with respect to the [010] direction of adjacent crystals. For bicrystal fabrication, single crystals of 10 mol% $Y_2O_3$-doped cubic $ZrO_2$ grown by the skull melting process (Earth Chemical Co. Ltd., Tokyo, Japan) were used. From ICP chemical analyses, it was found that the YSZ single crystals contained the following impurities: : $HfO_2$ < 1.42 wt%, $Na_2O$ < 190 ppm, CaO

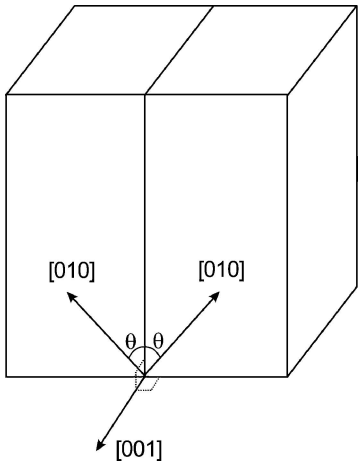


*Figure 1* Schematic illustration of a YSZ bicrystal fabricated in this study.

< 50 ppm, and $SiO_2$ < 14 ppm. The single crystals with the above-mentioned rotation axis and tilt angle were mechanically cut, and all surfaces were mechano-chemically polished by colloidal silica to obtain mirror state. The two single crystals were set so as to face the grain boundary planes with each other, and were joined by diffusion bonding at 1873 K for 15 h. It was confirmed that YSZ bicrystals thus obtained did not contain voids or cracks at the grain boundaries by optical microscope observations, indicating successful joining of the bicrystals.

In order to characterize the atomic structure of the YSZ grain boundary, TEM specimens were made from the YSZ bicrystals by the standard sample preparation techniques of mechanical grinding to a thickness of 0.1 mm, dimpling to 20 $\mu$m and Ar-ion beam milling at about 4 kV to obtain electron transparency. HRTEM observations were carried out with a JEOL 4010 operated at 400 kV with a point-to-point resolution of about 0.14 nm.

For SIMS measurements, YSZ bicrystals were cut into thin plates, as shown in Fig. 2a. In this case, the grain boundary plane was set about less than 20 $\mu$m away from the nearest specimen surface. All surfaces

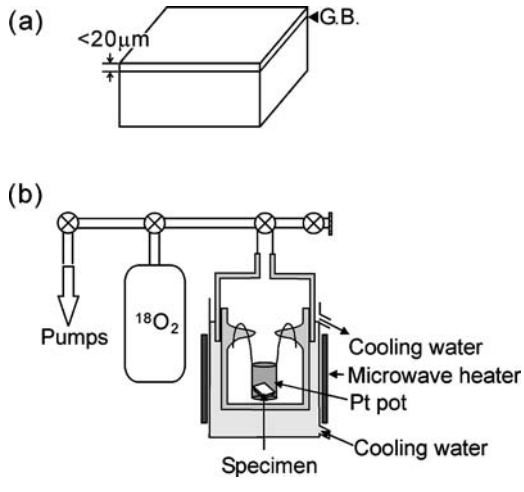


*Figure 2* (a) The shape of the specimen for SIMS measurement and (b) apparatus of $^{18}O$ isotope exchange for YSZ bicrystals.

of the thin plates were then polished by diamond paste to obtain mirror finish. Subsequently, the samples were annealed in the exchange apparatus (see Fig. 2b) at 550°C for 60 min to introduce $^{18}O$ isotopes from the surfaces.

$^{18}O$ depth profiles were measured across the $\Sigma 5$ boundary using a secondary ion mass spectrometry (CAMECA IMS-4F) with $^{133}Cs^+$ as the primary ion, an accelerating voltage of 10 kV and a beam current of 20 nA. To prevent charge-up at sample surfaces, Au metals were coated and the normal induced electron gun was used. Secondary ion intensities of $^{16}O^-$ and $^{18}O^-$ ($I(^{16}O^-)$ and $I(^{18}O^-)$) in the direction perpendicular to the grain boundary plane were measured, and the $^{18}O$ fraction ($C$) was calculated as

$$C = \frac{I(^{18}O^-)}{I(^{16}O^-) + I(^{18}O^-)}. \quad (1)$$

A final crater depth was determined using a Dektak 3030 profilometer.

## 3. Results and discussion

Fig. 3 shows the HRTEM image of the $\Sigma 5$ grain boundary fabricated in this study. White dots in this image correspond to the Zr atomic columns along the [001] direction, which was confirmed from HRTEM multi-slice simulations for bulk cubic zirconia viewed along [001] [11]. Neither disordered nor amorphous-like structures were observed around the boundary, indicating that the boundary is successfully joined at the atomic level.

From the magnified image in Fig. 3b, it can be seen that white dots at the boundary are arranged in a relatively symmetric manner with respect to the boundary plane. Therefore, this boundary is a symmetric one even at the atomic level, and the boundary core can be described by repeated arrangement of the symmetric structural units. Fig. 3c shows a rigid atomic structure model of the boundary, which was obtained by superpositioning the atomic columns of c-$ZrO_2$ on the observed image. Although the rigid model was constructed from the fact that white dots in the experimental image mean Zr columns, it should be noted here that $ZrO_2$ is consisted of Zr and O sublattices, which results in the situation that two O columns are located closely within the structural unit. Such close proximity of like-charge ions should make the grain boundary unstable due to significant electrostatic repulsion between like-charge ions, and thus structural relaxation is expected to occur at the boundary core. In addition, the real $\Sigma 5$ boundary observed here contains substitutional $Y^{3+}$ ions, which may affect the detailed core structure. In order to address this issue, atomistic or first-principles calculations should be applied to this boundary, which is beyond the scope of this study and will be reported elsewhere.

Since $Y^{3+}$ ions are doped in the $ZrO_2$ lattice by substituting for Zr ions, they may segregate at the boundary, and affect oxygen diffusivity across the boundary. In order to investigate $Y^{3+}$ segregation behavior at the $\Sigma 5$ boundary, energy-dispersive X-ray analyses (EDS) were performed, using an electron probe of about 1 nm. Fig. 4 shows EDS spectra taken (a) at the grain boundary and (b) from the grain interior. Relative intensities of Y-K$\alpha$ and Zr-K$\alpha$ lines ($= I(Y_{K\alpha})/I(Zr_{K\alpha})$) was found to be 0.41 at the $\Sigma 5$ boundary, which was larger than that ($I(Y_{K\alpha})/I(Zr_{K\alpha}) = 0.31$) in the grain interior, This indicates that the amount of $Y^{3+}$ ion content is higher at the boundary than in the bulk. $Y^{3+}$ segregation actually takes place at the $\Sigma 5$ boundary. According to previous experimental studies by Aoki *et al.*, Si segregation may have a significant effect on oxygen diffusion across grain boundaries of zirconia, but Si segregation was not explicitly detected in the present study.

In order to investigate oxygen diffusion behavior across the $\Sigma 5$ boundary, $^{18}O$ penetration profiles across the boundary plane were measured by the SIMS technique. For comparison, the $^{18}O$ profile in YSZ single crystals was also investigated in the same

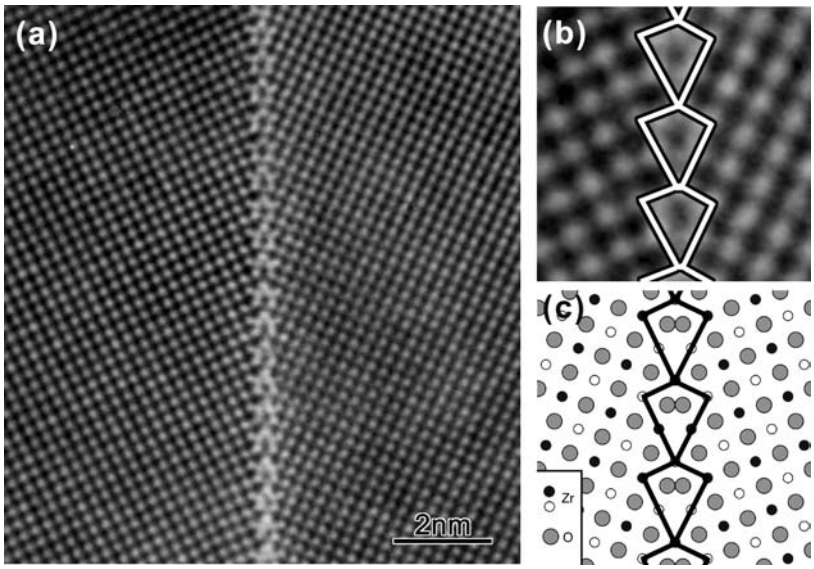


*Figure 3* (a) HRTEM image of the $\Sigma 5$ grain boundary viewed along the [001] direction. (b) the magnified image of the core structure of the grain boundary, and (c) the rigid structure model for the $\Sigma 5$ boundary.

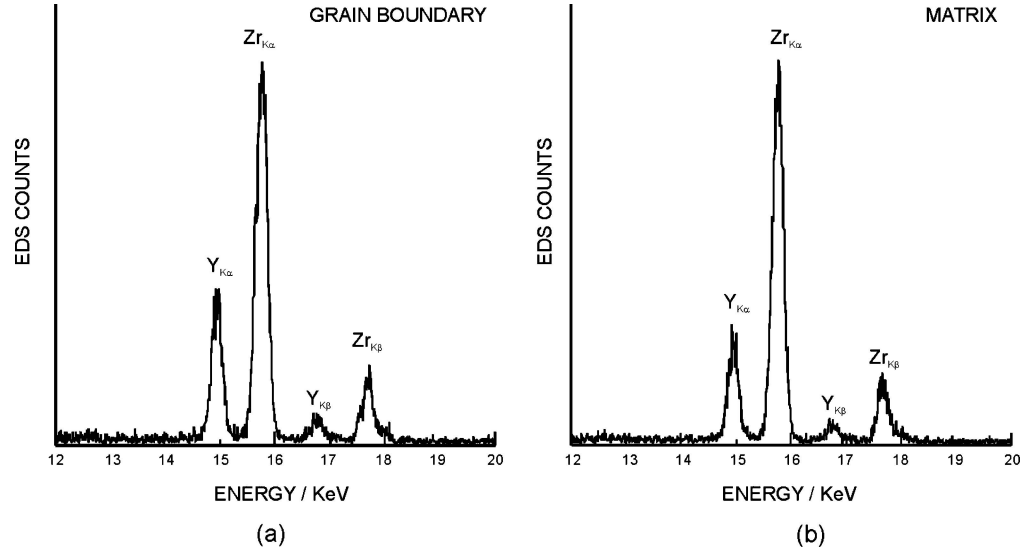


*Figure 4* EDS spectra taken from (a) the grain boundary and (b) the grain interior.

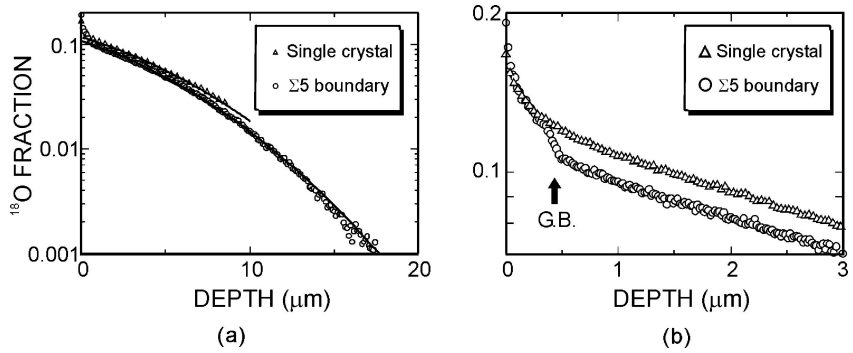


*Figure 5* (a) $^{18}$O depth profiles for the YSZ single crystals and the Σ5 bicrystals, and (b) the magnified profiles in the depth <3 $\mu$m, showing a abrupt decrease of $^{18}$O fraction at the grain boundary plane. The interpolated curves in (b) are obtained by fitting the data to analytical equations for grain boundary diffusion (see details in the text).

manner. Fig. 5a shows the thus obtained $^{18}$O profiles in a YSZ single crystal and across the Σ5 boundary, and (b) the magnified plots in the vicinity of the surface. In the single crystal, the $^{18}$O fraction profile smoothly decreased with increasing penetration depth. In contrast, the profile for the Σ5 boundary exhibits a similar curve in the depth range <0.4 $\mu$m with the one in the single crystal case, whereas the $^{18}$O fraction drops abruptly at around the depth of 0.4 $\mu$m (Fig. 5). This is considered to be due to the presence of the Σ5 boundary, indicating blocking of oxygen diffusion across the grain boundary.

In order to quantitatively estimate the grain boundary blocking effect, oxygen diffusion coefficients across the Σ5 boundary were evaluated by analyzing the measured $^{18}$O profiles based on mathematical treatments for grain boundary diffusion. Fig. 6 displays a schematic illustration representing $^{18}$O penetration behavior across the Σ5 grain boundary. In this case, the region $A$ corresponds to a single crystal area with a thickness of $d$, while $C$ is also a single crystal area with an infinite thickness. $^{18}$O is introduced from the surface of the region $A$, and diffuses into the region $C$ through the region $B$ with the Σ5 boundary. It was assumed here that the $A$ and $C$ regions have the same oxygen diffusion coefficient $D_O$, while an oxygen diffusion coefficient is $D'_O$ in the region B with a thickness of $\delta$.

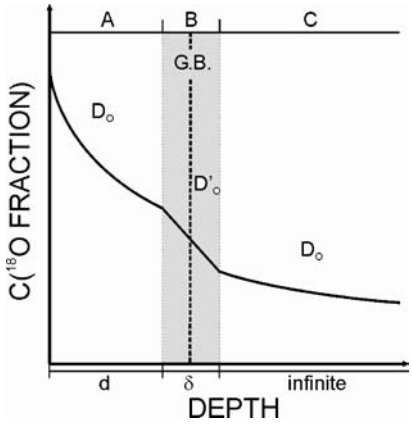


*Figure 6* Schematic geometry used for analytical treatments of oxygen diffusion across the grain boundary.

$^{18}$O is initially introduced from the surface by isotope exchange with $^{16}$O, and goes into the region $A$. Assuming rapid surface exchange reactions, the $^{18}$O penetration profile in the region $A$ can be represented by the following equation [19].

$$C'(x) = \frac{C(x) - C_{bg}}{C(x=0) - C_{bg}} = erfc\left(\frac{x}{2\sqrt{D_O t}}\right), \quad (2)$$

where $x$ is a penetration depth from the surface, $C_{bg}$ is a natural background level of $^{18}O$, and $t$ is an annealing time. At $x = d$ (the boundary between the regions $A$ and $B$), the concentration of $^{18}O$ can be thus represented by

$$C'(x = d) = erfc\left(\frac{d}{2\sqrt{D_O t}}\right) = erfc\left(\frac{d\sqrt{D'_O/D_O}}{2\sqrt{D'_O t}}\right). \quad (3)$$

Even in the region $B$, the $^{18}O$ concentration should change in the same manner as Equation 2, and thus $C'(x)$ in the range of $d \leq x \leq d+\delta$ is expressed as

$$C'(x) = erfc\left(\frac{d\sqrt{D'_O/D_O} + (x-d)}{2\sqrt{D'_O t}}\right) = erfc\left(\frac{d + (x-d)\sqrt{D_O/D'_O}}{2\sqrt{D_O t}}\right). \quad (4)$$

Also, from the boundary condition between $B$ and $C$ regions, $C'(x)$ in the range of $x \geq d + \delta$ is given by

$$C'(d+\delta) = erfc\left(\frac{d + \delta\sqrt{D_O/D'_O}}{2\sqrt{D_O t}}\right), \quad (5)$$

$$C'(x \geq d+\delta) = erfc\left(\frac{d + \delta\sqrt{D_O/D'_O} + \{x - (d+\delta)\}}{2\sqrt{D_O t}}\right) = erfc\left(\frac{x+s}{2\sqrt{D_O t}}\right), \quad (6)$$

where

$$s = \delta(\sqrt{D_O/D'_O} - 1). \quad (7)$$

From Equations 2 and 6, it can be seen that $C'(x \geq d + \delta)$ corresponds to $C'(x \leq d)$ shifted by $s$.

$D_O$ and $D'_O$ values for the $\Sigma 5$ boundary can be evaluated, by fitting the $^{18}O$ fraction data from the $\Sigma 5$ bicrystal to Equation 6. As can be seen in Fig. 5b, however, $^{18}O$ fractions in the vicinity of the specimen surfaces drastically decreased, and it was difficult to obtain $D_O$ by accurate fitting of the data in the narrow range of $x \leq 0.4$ $\mu$m by Equation 2. In order to obtain $D_O$ and $C(x = 0)$ more accurately, the $^{18}O$ profile for the single crystal in the depth range of 1 to 8 $\mu$m were fitted to Equation 2, where $D_O$ and $C(x = 0)$ are considered as variables. It was confirmed that the profile data were well fitted by the analytical curve of Equation 1, and $C(x = 0) = 0.12$ and $D_O$ of $6.91 \times 10^{-3}$ $\mu m^2$/sec were obtained (Fig. 5a).

In the similar way, the $^{18}O$ fraction data in the depth range of 1 to 8 $\mu$m from the $\Sigma 5$ bicrystal, which correspond to the region C in Fig. 6, were fitted by Equation 6 to obtain the value of $s$ in Equation 7. Here, the $C(x = 0)$ value of 0.12 obtained from the single crystal data was used. It was also well fitted by the theoretical curve (Fig. 5a), and the $D_O$ value was found to be $6.79 \times 10^{-3}$ $\mu m^2$/sec, which agrees well with that obtained above for the single crystal. Also, the profile shift $s$calculated was 0.74 $\mu$m. When $\delta$ was assumed to be 1.0 nm, the conventional G.B. thickness, a $D'_O$ value of $1.24 \times 10^{-8}$ $\mu m^2$/sec was calculated, which is smaller than $D_O$ by about 5 orders of magnitude.

## 4. Summary

YSZ bicrystals with the $\Sigma 5$ grain boundary were fabricated by diffusion bonding, and its atomic structure and $Y^{3+}$ segregation were investigated by HRTEM-EDS analyses. The results obtained can be summarized as follows.

(1) HRTEM observations showed that the $\Sigma 5$ boundary formed specific repeated structural units along the boundary without any voids and amorphous layers. From EDS analyses, it was found that Si impurities, which may play an important role for the grain boundary blocking of oxygen diffusion, were not detected around the grain boundary.

(2) SIMS measurements were performed for the $\Sigma 5$ bicrystals to study oxygen-diffusion behavior across the grain boundary plane. It was found that the oxygen profile exhibited an abrupt decrease around the boundary plane, indicating the oxygen-diffusion blocking of the $\Sigma 5$ grain boundary. Since the present $\Sigma 5$ boundary was a Si-free boundary, its grain boundary blocking effect must be an intrinsic feature arising from its core structure and/or yttrium segregation at the grain boundary.

## Acknowledgement

This work was supported by a Grant-in-aid for Scientific Research from the Japan Society for the Promotion of Science, and the Ministry of Education, Culture, Sports, Science and Technology of Japan.

## References

1. T. H. ETSELL and S. N. FLENGAS, *Chem. Rev.* **70** (1970) 339.
2. Y. ARACHI, H. SAKAI, O. YAMAMOTO, Y. TAKEDA and N. IMANISHAI, *Solid State Ion.* **121** (1999) 133.
3. F. BAUMARD and P. ABELARD, in "Advances in Ceramics, Science and Technology of Zirconia II," edited by A. H. Heuer and L. W. Hobbs (American Ceramic Society, Columbus, OH, 1984) Vol. 3, p. 555.
4. S. P. S. BADWAL and J. DRENNAN, *J. Mater. Sci.* **22** (1987) 3231.
5. H. L. TULLER, *Solid State Ion.* **131** (2000) 143.
6. P. MONDAL and H. HAHN, *Ber. Bunsenges Phys. Chem.* **101** (1997) 1765.
7. I. KOSACKI, B. GORMAN and H. U. ANDERSON, in "Ionic and Mixed Conductors" (Electrochemical Society, Pennington, NJ, 1998) Vol. III, p. 631.
8. M. AOKI, Y.-M. CHIANG, I. KOSACKI, J.-R. LEE, H. L. TULLER and Y. J. LIU, *J. Am. Ceram. Soc.* **79** (1996) 1169.
9. X. GUO, W. SIGLE, J. FLEIG and J. MAIER, *Solid State Ion.* **154–155** (2002) 555.
10. X. GUO, *ibid.* **81** (1995) 235.
11. N. SHIBATA, F. OBA, T. YAMAMOTO, Y. IKUHARA and T. SAKUMA, *Phil. Mag. Let.* **82** (2002) 393.
12. N. SHIBATA, F. OBA, T. YAMAMOTO and Y. IKUHARA, *Phil. Mag.* **84** (2004) 2381.

13. E. C. DICKEY, X. FAN and S. J. PENNYCOOK, *J. Am. Ceram. Soc.* **84** (2001) 1361.
14. W. D. KINGERY, D. C. HILL and R. P. NELSON, *ibid.* **43** (1960) 473.
15. V. S. STUBICAN and J. W. OSENBACH, *Solid State Ion.* **12** (1984) 375.
16. L. A. LIMSON and R. E. CARTER, *J. Am. Ceram. Soc.* **49** (1966) 139.
17. W. K. CHEN and N. L. PETERSON, *ibid.* **60** (1980) 566.
18. A. ATKINSON and R. I. TAYLOR, *Phil. Mag.* **43** (1981) 979.
19. J. CRANK, in "The Mathematics of Diffusion," 2nd edn. (Oxford Univ. Press, 1975) p. 28.

*Received 31 August 2004*
*and accepted 31 January 2005*